02

# Photocatalytic Reaction $NO+CO\xrightarrow{h\nu}(CO_2)_{ads}+1/2N_2$, activated on $ZnO/ZnO_{1-x}/O^-$ under exciton resonance excitation

© I.V. Blashkov, V.V. Titov

Fock Institute of Physics, St.Petersburg State University,
198504 Petrodvorets, Russia

e-mail: i.blashkov@spbu.ru

*Received 01.07.2022*
*Revised 19.09.2022*
*Accepted 23.09.2022*

The exciton channel of ZnO photoactivation was used for the first time to carry out the environmentally important photocatalytic reaction $NO+CO\xrightarrow{h\nu}(CO_2)_{ads}+1/2N_2\uparrow$ on ZnO. When the excitation energy is delivered to the surface by an electrically neutral exciton, there are no losses in recombination and in overcoming the potential surface barrier, which are the main losses in the transfer of photo-generated $e^-/h^+$ pairs. To suppress the undesirable radiative decay of an exciton, the $ZnO/ZnO_{1-x}/O^-$ 2D structure was created on the ZnO surface, in which the exciton decays nonradiatively into a pair of long-lived local states of an electron and a hole, on which the reactionary acts occur. For the redox reaction (1), the obtained values of the quantum yield $Y$ (the number of reaction acts per one absorbed quantum) and the efficiency $E$ (the number of acts per one incident quantum) upon exciton excitation at $\lambda = 382$ nm are 5−7 times greater than when excited in the interband absorption region at $\lambda = 365$ nm. The methods of mass-spectrometry (MS) and thermodesorption spectroscopy (TDS) were used to study the initial, intermediate and final products of reaction (1) in the gas and adsorbed phases, and the features of the influence of the initial products NO and CO on each other during the interaction of their mixture with ZnO in the dark and under irradiation at $\lambda = 382$ nm.

**Keywords:** photocatalysis, exciton, 2D structure $ZnO/ZnO_{1-x}/O^-$, long-lived active centers, redox reaction, air purification.

DOI: 10.21883/0000000000

## 1. Introduction

In recent years, ZnO has occupied one of the leading positions among semiconductor photocatalysts. Photocatalysis on ZnO is effective in the degradation of a wide range of organic and inorganic pollutants into biodegradable or less toxic organic compounds [1].

Features of the electronic structure of ZnO — large band gap (3.37 eV at 300 K) with electronic affinity $\sim 4.0$ eV, high carrier mobility ($200\,cm^2/V{\cdot}s$ at 300 K [2]) — made ZnO the most active (along with $TiO_2$) photocatalyst of redox reactions. However, the photoactivation of ZnO requires ultraviolet (UV) radiation, the proportion of which in the solar spectrum does not exceed $\sim 5\%$. To shift the spectrum of ZnO activity to the visible region, various methods of sensitization of ZnO are used by doping with metals and nonmetals [2–5], organic sensitizers, the formation of heterostructures with narrow-band semiconductors [2,6,7].

Earlier, for the first time, we used the absorption of intrinsic anionic and cationic vacancies (centers of types F and V, respectively) to self-sensitize ZnO to the visible region of the spectrum [8,9]. The study showed that the quantum yield of the reaction

$$NO + CO + h\nu \rightarrow CO_2 + 1/2N_2 \qquad (1)$$

when illuminated with light, the visible range is almost an order of magnitude greater than when illuminated in the UV range. However, the efficiency of visible light remained low due to weak absorption by the sample. The task was set [10] to increase the quantum yield in the region of intrinsic absorption of ZnO.

The main reason for the decrease in the quantum yield of the reaction during activation in the UV region is — loss of carriers when moving to the surface centers of photocatalysis due to paired recombination $e^- - h^+$ and recombination with recombination centers. In addition, the surface potential barrier, facilitates the exit of carriers of one sign to the surface, delays carriers of the opposite sign.

After the discovery of a neutral excited particle in crystals, named exciton [11], A.N. Terenin suggested using it for activation catalytic reactions on semiconductor crystals instead of charge carriers [12]. Thus, the losses mentioned above can be significantly reduced if excitons are used to transfer the excitation energy. The uniquely high binding energy of excitons in ZnO is 60 meV, that ensures the stability of $e^-/h^+$ pairs during their transfer at room temperature ($kT = 27$ meV). However, the exciton decays radiatively on the surface, and the enclosed energy is carried away in the form of exciton luminescence. Apparently, for this reason, the activity of excitons in photocatalysis on semiconductors has not been experimentally confirmed until recently [13]. We have been looking for an opportunity to suppress the radiation exciton decay channel [14]. It was shown [15] that surface photoluminescence (PL) on ZnO can be

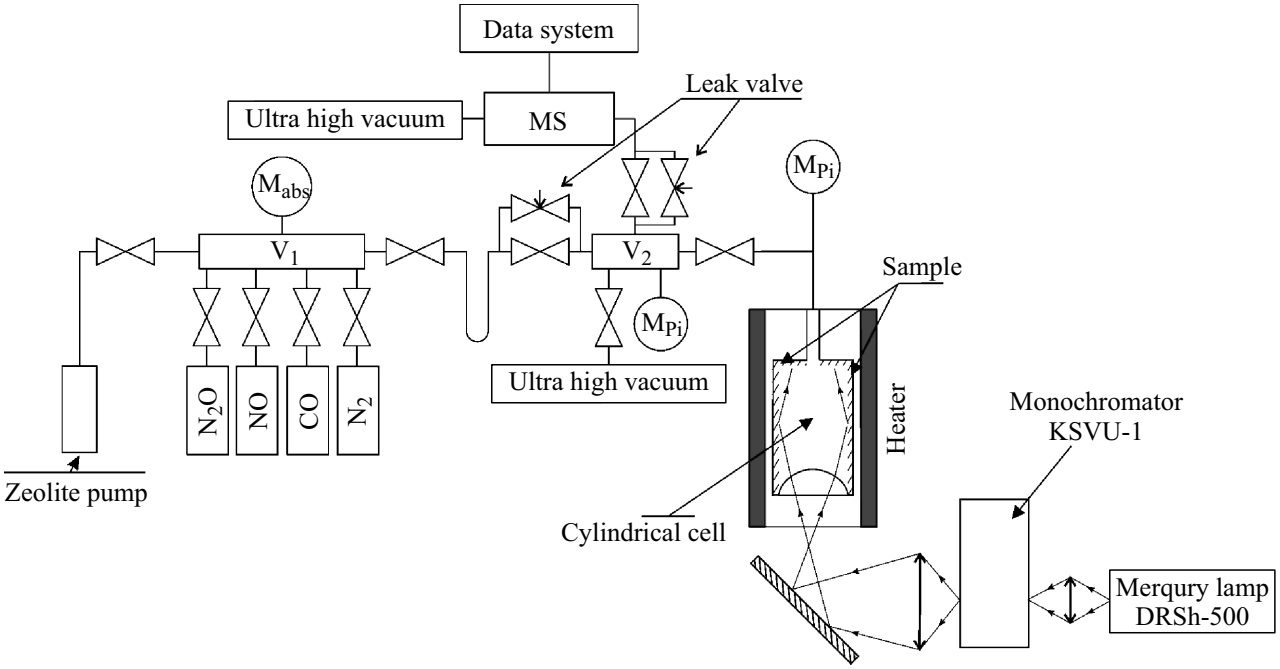


**Figure 1.** Experimental setup: $M_{Pi}$ —Pirani pressure gauge, $M_{abs}$ — absolute pressure gauge, MS — mass spectrometer, $V_2$ — volume for the preparation of a gas mixture.

suppressed by special treatment in an oxygen atmosphere. In this work, the electrophysical parameters of the sample *in situ* were controlled by UV spectroscopy (UPS) (8.43 eV) (values of the Schottky barrier, the dipole layer of adsorbed oxygen, the surface bending of zones). The sequence of oxidation cycles was carried out in combination with dosed photoreduction of the surface layer by photodesorption of oxygen in ultrahigh vacuum (the amount of photodesorbed oxygen was controlled by a mass spectrometer). It was shown that as a result of such a procedure, a surface submonolayer 2D structure $ZnO/ZnO_{1-x}/O^-$ is formed, effectively suppressing exciton PL. In such a 2D structure, the exciton is not emitted, but decays into a pair of long-lived ones (up to $8 \cdot 10^3$ s) electron-donor and hole centers, on which the redox reaction [13] occurs place.

Indeed, using the example of photo-activated isotope exchange (POIE) of oxygen, which is used as a model of redox reactions, it is shown that the efficiency of the $ZnO/ZnO_{1-x}/O^-$ structure when activated in the region of resonant exciton excitation is approximately 8 times higher than in the region of interband absorption [10]. The specificity of the reaction of the POIE test is that it proceeds in the binary system $O_2-ZnO$, and the photocatalyst is not affected by the initial, intermediate and final products. However, is it possible to carry out a redox reaction in real conditions?

The study of this issue has become the purpose of this work. We have chosen the environmentally important reaction $NO + CO \xrightarrow{h\nu} CO_2 + 1/\ 2N_2 \uparrow$, previously investigated by us when ZnO is excited in visible region of self-sensitization [8]. For comparison, the interband excitation region ($\lambda = 365$ nm) and the exciton resonance excitation band ($\lambda = 382$ nm) were used.

## 2. Experimental techniques and methods

In this paper, the reaction was studied by photomanometry, kinetic photomass spectrometry in the gas phase and thermoprogrammable desorption (TPD) with mass analysis of the desorbed gas [8]. The diagram of the experimental setup is presented in Fig. 1.

In the previous work, we used a measuring cell in the form of a Dewar cylinder with a poured sample of ZnO weighing 5.6 g. It was found that in such a scheme, the efficiency of the reaction was limited by the diffusion of intermediate and final products through the sample. Therefore, in this work, a sample with a smaller mass (about 300 mg) was applied as a thin layer. The sample ZnO „High Purity 12-2“ was deposited from an aqueous suspension on the walls of a cylindrical quartz measuring cell ($h = 40$ mm, $d = 15$ mm), the layer thickness was 15 mg/cm$^2$. Before the experiments, the sample was prepared as follows: heating in an oxygen atmosphere to 823 K→ cooling down to 673 K→ evacuation at 673 K→ cooling down to room temperature → exposure of the sample to $\lambda = 365$ nm ($I_{365} \approx .10^{16}$ photons cm$^{-2}$s$^{-1}$, $t \approx .10$ min)→ short-term oxygen admission ($P = 0.1$ Torr)→ heating up to 473 K in vacuum.

Ultraviolet illumination led to photodesorption of molecular oxygen from the surface and photodestruction of the surface layer due to photodesorption of structural oxygen. The amount of photodesorbed molecular oxygen from the

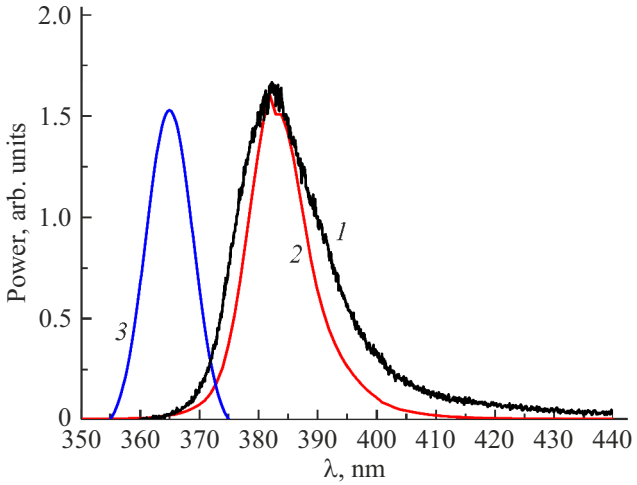


**Figure 2.** Spectra: *1* — exciton resonance excitation PL [10]; *2* — LED emission with a maximum of $\lambda = 382$ nm taking into account the absorption of the sample; *3* — DRSH-500 radiation with a maximum of $\lambda = 365$ nm, isolated by a monochromator KSVU-1.

adsorbed layer and atomic oxygen from the surface layer of the structure was determined mass spectrometrically [14]. As a result of partial reduction, band bending was formed on the surface. Subsequent oxygen adsorption leads to the formation of a 2D structure on the surface of $ZnO/ZnO_{1-x}/O^-$, which is a pit bounded on the inner side of the surface by a Schottky barrier, and on the outer side by a field of strongly bonded atomic oxygen. It is in this quantum-dimensional 2D structure that the exciton decays nonradiatively into a pair of long-lived centers [15].

The composition of the gas phase and desorption products was controlled using a monopole mass spectrometer APDM-1 (MS). The residual vacuum in the reactor was no worse than $P = 10^{-7}$ Torr. The use of an absolute pressure gauge for calibration made it possible to obtain results in absolute units [molecules $s^{-1}$ $cm^{-2}$] for flows and [molecules $cm^{-2}$] for coatings. The reactor is equipped with a heater that allows linear heating for measurements of thermal desorption (TD) spectra and heat treatment of the sample.

The XRD analysis showed that the sample consists of 100% of the wurtzite phase. According to the analysis by differential ultrasonic spectroscopy and scanning electron microscopy, the sample particles are conglomerates of crystallites with a size of 100 nm. The sample area by the BET method (by adsorption $N_2$) was 20.3 $m^2/g$ [8].

The sample was irradiated with two sources: The UV LED RF-UVXC35LN-UD (Refond) with a radiation maximum of $\lambda = 382$ nm, which corresponds to the resonant exciton excitation band, and a high-pressure mercury lamp DRSH-500 with a monochromator KSVU-1 ($\lambda_{max} = 365$ nm), which corresponds to the interband excitation of the ZnO sample. The intensity of incident radiation in both cases, measured by a calibrated photocell F17, was $\approx 10^{16}$ photons $cm^{-2}s^{-1}$.

Absorption Spectrum $(1 - R)$ of the sample $ZnO/ZnO_{1-x}/O^-$ used in the experiment is given in our previous work [10]. The radiation spectrum of the LED absorbed by the sample lies inside the region of resonant exciton excitation at room temperature (Fig. 2, curves *1* and *2*). The curve *3* in Fig. 2 represents the emission spectrum of the used mercury lamp DRSH-500 with $\lambda = 365$ nm. Thus, the spectra of the two selected radiation sources overlap only slightly in the region of 365–375 nm. We note that the molecules of both NO and CO do not absorb activating UV radiation and, therefore, do not distort the studied spectrum of photoactivation.

## 3. Results

### 3.1. Kinetic dependences of dark and photostimulated interactions of NO, CO and mixtures of NO + CO with ZnO

***Photocatalytic reaction*** $NO + CO \xrightarrow{h\nu} (CO_2)_{ads} + 1/2N_2$. Fig. 3 shows the dependences of the concentrations of reagents and reaction products (1) on the irradiation time by $\lambda = 382$ nm ($a$) and by $\lambda = 365$ nm ($b$). The admixture of NO + CO is accompanied by rapid dark adsorption of both gases with the release into the gas phase $N_2O$. The illumination is turned on shortly before full adsorption NO.

The release of $N_2$ begins after the completion of photoadsorption of NO only in the presence of CO in the gas phase. The character of the kinetic curves of CO and NO is typical for the initial reaction products, and $N_2$ — for the final one. The second final product — $CO_2$ is not detected in the gas phase, it accumulates in the adsorbed state. The kinetic curve of $N_2O$ release a maximum in the middle part, which is typical for intermediates.

Since NO was almost completely adsorbed under dark conditions (Fig. 3, $a$), the second stage of the reaction (1) — the release of molecular nitrogen $N_2$ into the gas phase was chosen for a comparative analysis of kinetic parameters. On Fig. 4 the allocation processes are presented $N_2$ ($a$) and $N_2O$ ($b$), under irradiation $\lambda = 365$ and 382 nm. The reaction (1) proceeds upon irradiation both at $\lambda = 382$ nm and at $\lambda = 365$ nm. The region of pressure drops area $N_2O$ ($\lambda = 382$ nm) is well described by an exponential function, which indicates the first order of the reaction.

For a quantitative comparison of the efficiencies of $\lambda = 365$ nm and $\lambda = 382$ nm, the initial linear section of the kinetics of $N_2$ is selected (Fig. 4, $a$, black lines). The efficiency and quantum yield of the reaction (1) under irradiation at $\lambda = 382$ nm is 5–7 times greater than at $\lambda = 365$ nm.

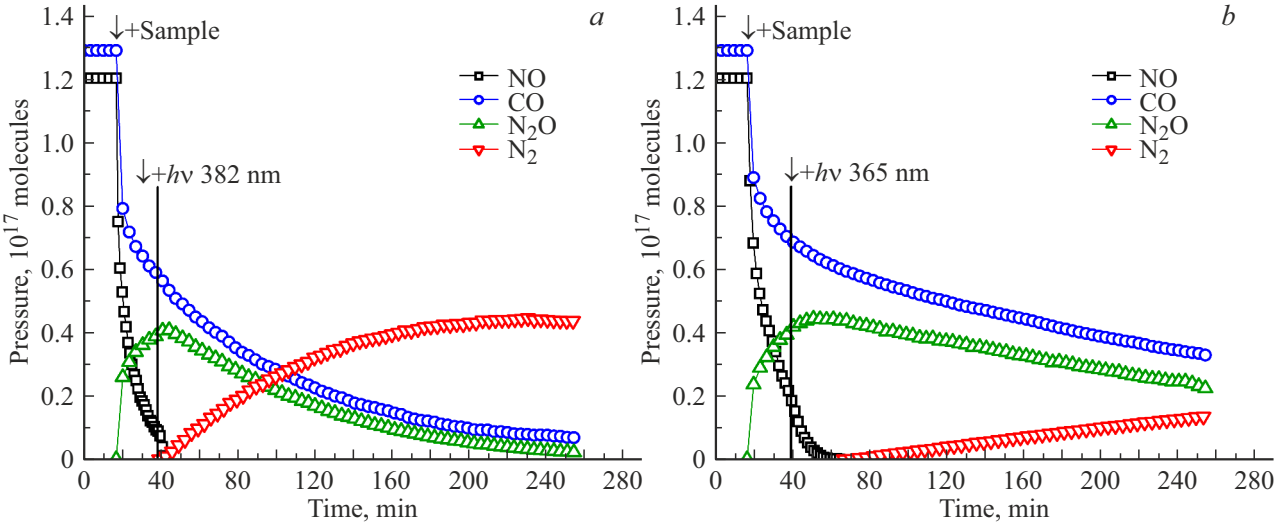


**Figure 3.** Dependences of concentrations of reagents and reaction products (1) on time on $ZnO/ZnO_{1-x}/O^-$ under irradiation (*a*) $\lambda = 382$ nm, (*b*) $\lambda = 365$ nm ($T = 300$ K, $P_0(NO) = P_0(CO) = 0.05$ Torr). Incident radiation intensity: $I_{382} = I_{365} = (3-5) \cdot 10^{16}$ photons cm$^{-2}$ s$^{-1}$.

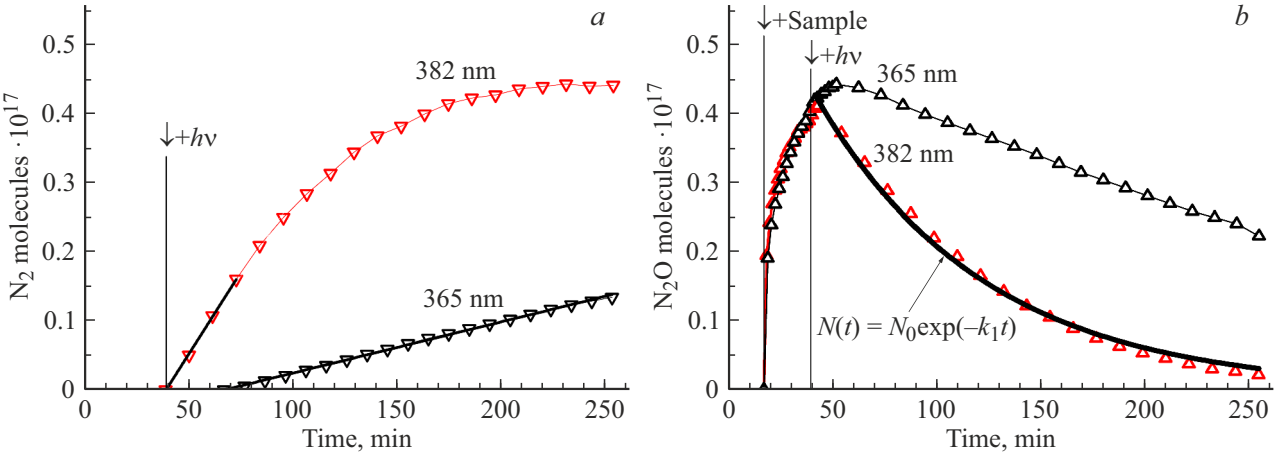


**Figure 4.** Release into the gas phase (*a*) $N_2$ and (b) $N_2O$ in the reaction (1) at $\lambda = 382$ and 365 nm. The illumination of the samples is the same in both cases.

***Dark and photostimulated interactions of NO with ZnO.*** At room temperature, NO is adsorbed on the sample (Fig. 5), the release of $N_2O$ into the gas phase is not observed. Illumination (Fig. 5) causes intense photoadsorption of NO and the release of $N_2O$ (Fig. 5). The subsequent 30 min illumination did not lead to the appearance of $N_2$, despite the fact that NO was completely photoadsorbed, and the pressure of $N_2O$ reached a maximum.

***Dark and photostimulated interactions of NO with ZnO in the presence of CO.*** Fig. 6 shows the kinetic dependences of the concentrations of reagents and products of dark adsorption of NO without CO and in a mixture of NO + CO. The addition of CO to the mixture to NO significantly accelerates the adsorption of NO and leads to a noticeable release of $N_2O$ into the gas phase.

Fig. 7 shows the separation of the stages of photoadsorption of NO and subsequent photoreaction of CO with photoadsorbed NO. At interval 1, NO was completely photoadsorbed ($\lambda = 382$ nm), and in the gas phase, $N_2O$ appeared in the amount of $\sim 30\%$ (in terms of content N) from the initial amount of NO.

After pumping out $N_2O$ at interval 2, the sample was illuminated in the atmosphere of CO. The release of NO molecules displaced from the adsorption centers by CO molecules is noticeable. $N_2O$ is released into the gas phase five times weaker than at interval 1. This correlates with the ratio of NO pressures at the first and second stages and shows that NO is consumed mainly from the gas phase for the formation of $N_2O$, although up to 65% of nitrogen-containing forms formed at interval 1 are adsorbed on the sample. Irradiation in CO (Fig. 7, stage 2) leads to the

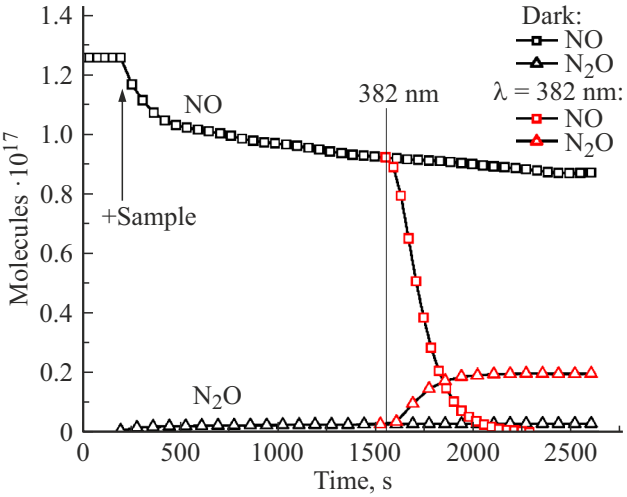


**Figure 5.** Kinetic curves of dark adsorption and photoadsorption ($\lambda = 382$ nm) NO on ZnO ($P_0(\mathrm{NO}) = 0.05$ Torr).

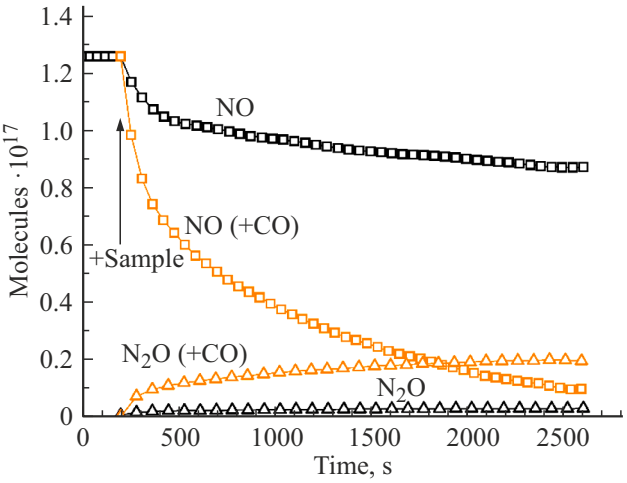


**Figure 6.** Kinetic curves of dark adsorption of NO and NO in a mixture of NO + CO ($P_0(\mathrm{NO}) = P_0(\mathrm{CO}) = 0.05$ Torr) on ZnO.

release of $N_2$ into the gas phase, however, at a much lower rate than when irradiating a mixture of NO + CO (Fig. 3, *a*). There are traces of $N_2$ in the gas phase.

At stage 3, photoadsorption of NO is slightly weaker than at interval 1. In the gas phase, $N_2O$ is allocated and (in contrast to the interval 1) $N_2$. As it follows from this experiment that for the most effective reduction of NO to $N_2O$ and then $N_2O$ to $N_2$, a combination of illumination and the presence of CO in the gas mixture is necessary.

### 3.2. Analysis of the adsorbed phase after interactions of NO, CO and a mixture of NO,+,CO with ZnO by TPD spectroscopy

Thermoprogrammable desorption (TPD) with mass spectrometric analysis of the desorbed phase was used to analyze the composition and binding energy of the adsorbed intermediate and final products. This method uses the Wigner–Polyany equation for the desorption rate:

$$-\frac{d\theta}{dt} = k\theta^n = Ae^{-\frac{E_a}{RT}}\theta^n, \qquad (2)$$

where $\theta$ — surface concentration of adsorbed molecules or degree of surface filling, $k$ — desorption rate constant, $A$ — pre-exponential factor, $E_a$ — activation energy, $R$ — universal gas constant, $T$ — thermodynamic temperature, $n$ — process order (1st or 2nd). In the TPD method, the rate of desorption of reaction products is measured with a linear increase in temperature: $T = T_0 + \beta t$, where $\beta$ — the heating rate (K/s).

$dt = \frac{dT}{\beta}$ we substitute (2) into the original equation:

$$-\frac{d\theta}{dT} = \frac{A}{\beta}e^{-\frac{E_a}{RT}}\theta^n. \qquad (3)$$

In the experiment, the desorption rate is determined mass spectrometrically by the flow of molecules from the sample in the flow reactor mode [16].

***Interaction of NO with ZnO.*** Fig. 8 shows the TD spectra of the products of dark and photostimulated adsorption of NO on ZnO (Fig. 5).

The low-temperature peak NO (peak *1*, $T = 345-350$ K) has an asymmetric shape characteristic of molecular desorption. The shape is modeled by a first-order peak with $\nu = 10^{12}$ s$^{-1}$, $E_{\mathrm{des}} = 0.92$ eV. Illumination reduces this peak of NO with a simultaneous increase in the amount of $N_2O$ in the gas phase (Fig. 5) without a noticeable increase in the amount of adsorbed $N_2O$, therefore, in Fig. 8, both peaks $N_2O$ correspond to a single curve. This indicates that the weakly bound form $NO^-$ is responsible for the formation of $N_2O$. In general, the TD spectrum of NO has a complex structure, which indicates a significant variety

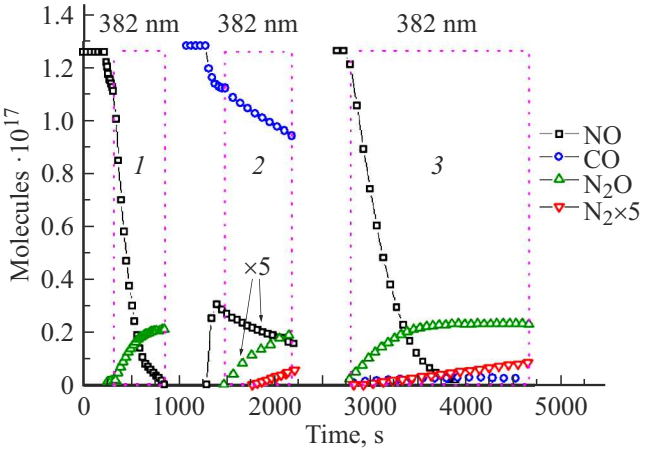


**Figure 7.** Kinetic curves obtained by irradiating a ZnO sample in: *1* — NO; *2* —$NO_{ads}$ + CO; *3* — $NO_{gas} + NO_{ads} + CO_{ads}$ with pumping out the remaining products in the gas phase at the end of each stage.

of forms of adsorption. Fourier-transform infrared spectroscopy with Fourier transform (FTIR) and MS showed the presence on the surface of $TiO_2$ of the forms $NO^-$, $NO_2^-$, $NO_3^-$, dimers $N_2O_2$, $N_2O_3$, $N_2O_4$ in neutral and negatively charged forms [17].

***Interaction of CO with ZnO.*** The admission of CO injection into the reactor with ZnO was accompanied by

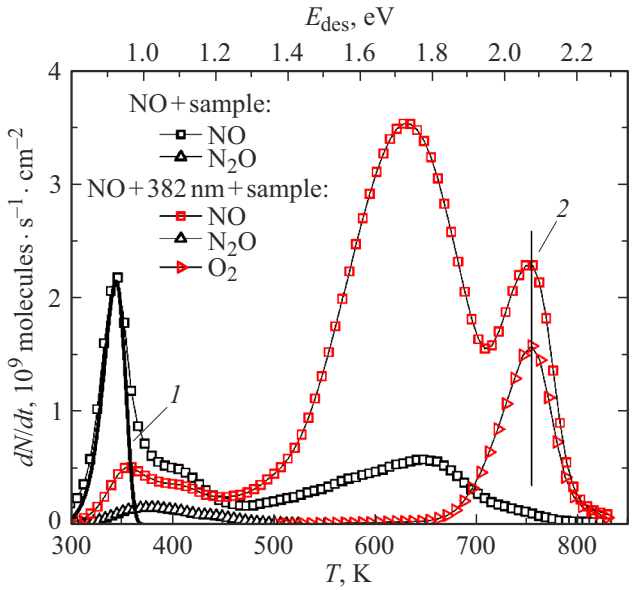


**Figure 8.** Thermal desorption spectrum of reaction products $NO + ZnO/ZnO_{1-x}/O^-$: *1* — first-order model peak ($\nu = 10^{12}\,s^{-1}$, $E_{des} = 0.92$ eV) desorption NO, *2* — peak NO, accompanied by a peak of molecular oxygen.

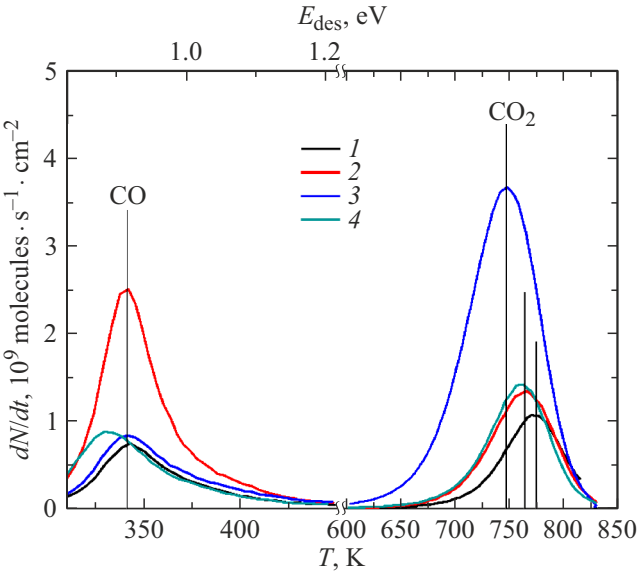


**Figure 9.** Thermal desorption spectra of products of dark and photostimulated interactions of CO with $ZnO/ZnO_{1-x}/O^-$: *1* — CO ($P_0 = 0.05$ Torr), *2* — CO ($P_0 = 0.1$ Torr), *3* — CO ($P_0 = 0.05$ Torr) + NO ($P_0 = 0.05$ Torr), *4* — CO ($P_0 = 0.05$ Torr) + 382 nm.

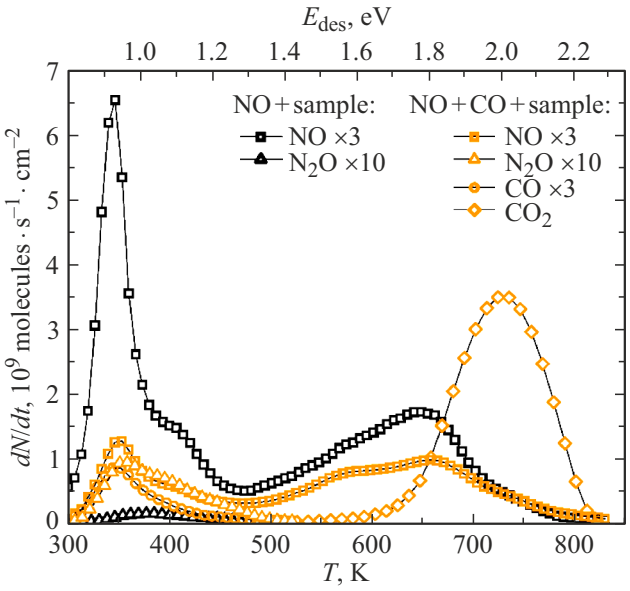


**Figure 10.** Thermal desorption spectra of reaction products $NO + ZnO/ZnO_{1-x}/O^-$ and $NO + CO\ ZnO/ZnO_{1-x}/O^-$.

rapid (within several tens of seconds) reversible adsorption. The illumination causes a slight increase in the rate of adsorption of CO without the release of $CO_2$ into the gas phase (Fig. 9).

The TD spectra show peaks of CO with a maximum of 340 K and $CO_2$ with a maximum at 750–780 K (Fig. 9). We have previously shown that irradiation of $TiO_2$ in CO induces absorption in the IR and visible regions due to conduction electrons and bands of monodentate (1450–1350 $cm^{-1}$) and bidentant (1570–1315 $cm^{-1}$) carbonates [18]. Similarly, when ZnO is illuminated in the CO atmosphere , bands of carboxylate CO appear$_2^-$ (band 1620 $cm^{-1}$) and carbonate $CO_3^{2-}$ (1570–1315 and 1450–1350 $cm^{-1}$) structures [19,20].

***Interaction of NO + CO with ZnO.*** Fig. 10 shows the TD spectra of the products of the interaction of NO with ZnO in the presence of CO and without it (Fig. 6).

In the presence of CO, an increase in the amount of $N_2O$ is observed both in the gas (Fig. 6) and in the adsorbed phases, correlating with a decrease in low-temperature forms of NO (Fig. 10).

***Interaction of NO + CO with ZnO under irradiation at $\lambda = 382$ nm.*** Analysis of the TD spectra of the adsorbed reaction products (1) (after pumping out the final products at the moment when the separation of $N_2$ is completed (Fig. 4, *a*)) showed that the main product of thermal desorption is $CO_2$ (fig. 11). In addition to $CO_2$, TD peaks NO, $N_2O$, CO were found. Their amount does not exceed 5–8% of the TD peak of $CO_2$. It has been established that the TD forms of peaks NO, $N_2O$ do not change during the entire time of ZnO illumination in a

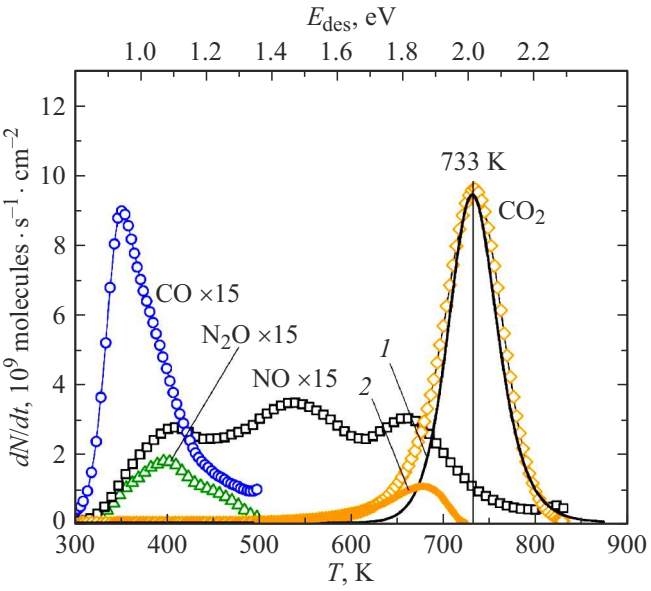


**Figure 11.** Thermal desorption spectrum of reaction products after irradiation $\lambda = 382$ nm. *1* — model peak of $CO_2$ of the second order with $E_{des} = 2.47$ eV, *2* — difference between experimental peak and model peak *1*. The scale $E_{des}$ in the upper part is calculated for first-order desorption with $\nu = 10^{12}$ $s^{-1}$ and does not apply to the peak of $CO_2$ of the second order.

mixture of NO + CO, which allows us to consider them as by-products of the reaction (1).

## 4. Discussion

The kinetic data obtained are agree with the previously proposed two-stage redox reaction mechanism (1) [8]. The primary photophysical stage of photoactivation of the system includes exciton photogeneration, its drift to the surface and nonradiative decay into a pair of long-lived centers — electron donor centers F, $F^+$, $Zn^+$ and hole centers V, $V^-$. These are the centers that interact with NO and CO molecules on the surface. The first stage, i.e. the reduction of NO to $N_2O$, is described by the reaction

$$CO + 2NO \xrightarrow{h\nu} CO_2 + N_2O, \qquad (4)$$

where $N_2O$ is an intermediate product, as indicated by the specific shape of its kinetic curve having a maximum.

In the second stage, $N_2O$ is restored to $N_2$:

$$CO + N_2O \xrightarrow{h\nu} CO_2 + N_2 \uparrow . \qquad (5)$$

The difference between the reactions carried out in this work and in the work of [8] consists in the primary act of photoactivation. In the work [8], photoactivation was used in the absorption of intrinsic structural defects of F- and V-types. This made it possible to obtain a quantum yield $Y$ higher than in the interband absorption region, due to an increase in the illuminated surface of the powder catalyst (the absorption coefficient is $k$ small) and the creation of long-lived active centers. However, the efficiency of $E$ photoactivation was lower than in the interband absorption region due to the low concentration of structural defects.

In this paper, an attempt is made to combine a high exciton absorption coefficient with a high efficiency of excitation energy transfer to chemical reagents by reducing energy transfer losses in a solid. For this purpose, an electrically neutral exciton was chosen as an energy carrier. The exciton does not lose energy for recombination of the electron and the hole and for overcoming electrical barriers, as it occurs during interband absorption. Radiation losses and decay in the field of the surface barrier are minimized by the surface 2D structure $ZnO/ZnO_{1-x}/O^-$. As shown in [15], in this structure the exciton decays into a pair of electron-donor and hole centers. The study of the POIE reaction, which is a model for the redox reaction, confirmed that the efficiency of photoactivation in the exciton region is higher than in the interband absorption region. In the case of nonradiative exciton decay, the same long-lived centers are formed in the 2D structure, apparently, as in the case of resonant excitation of F- and V-type centers [8]. According to the spectra of thermally stimulated luminescence [13], they are identified as centers of F and V types. It is at such centers that the reaction (1) takes place.

The primary photophysical act of excitation of a catalyst in interaction with an exciton:

$$\mathrm{exc}(e^- + h^+) + Zn^{2+}O^{2-} \rightarrow Zn^+ + O^-. \qquad (6)$$

Further, the reaction is $NO + CO \xrightarrow{h\nu} CO_2 + 1/2N_2$ proceeds in 2 stages according to the scenario [8]. The first stage is characterized by photoadsorption of the initial products to form $CO_{2(ads)}$ and reduction of NO to $N_2O$ (reaction (4)). NO reactions with photogenerated media:

$$NO_{ads} + Zn^+ \rightarrow NO^- + Zn^{2+}, \qquad (7)$$

$$Zn^{2+} + O^- + NO \rightarrow Zn^+ + NO_2^- + F^+. \qquad (8)$$

After the photoadsorption of NO is completed, the second stage begins: the reduction of the intermediate $N_2O$ to $N_2$ (reaction (5)). The final product $CO_2$ remains in the adsorbed state and can be thermally extracted in a stoichiometric ratio.

Secondary reactions in the adsorbed phase are discussed in [8] and are given in the Appendix.

The efficiency and quantum yield calculated with respect to the release of molecular nitrogen into the gas phase at the second stage of the reaction (1) (Fig. 3, 4) turned out to be 5–7 times higher when irradiated on the exciton band with $\lambda_{max} = 382$ nm compared to the area of interband absorption — band with $\lambda_{max} = 365$ nm.

In the conducted experiments (Fig. 3, 5–7) acceleration of NO adsorption was observed with simultaneous release of $N_2O$ both when the sample illumination was turned on and when CO was added to the mixture. A qualitative dependence has been established (Fig. 7) of the efficiency

of reducing NO to $N_2O$ and then $N_2O$ to $N_2$ on the combination of illumination conditions and the amount of CO in the gas mixture NO + CO.

As a result of photoadsorption of NO, two broad peaks are formed in the range $500\,\mathrm{K} < T < 800\,\mathrm{K}$ (Fig. 8). With the $\sim 95\%$ accuracy, it was possible to simulate the obtained spectrum with second-order desorption peaks with $E_{\mathrm{des}} = 1.65\,\mathrm{eV}$, 1.82 eV, 1.99 eV, 2.14 eV, respectively, and a first-order desorption peak at $T = 755\,\mathrm{K}$ with $E_{\mathrm{des}} = 2.07\,\mathrm{eV}$. The high-temperature peak of NO desorption is accompanied by the peak of molecular oxygen identical in shape and the position of its maximum. This indicates a single source of both peaks at 755 K, which may be the result of a dissociative desorption of $NO_3^-$ nitrates, as evidenced by the asymmetric shape of peak 2. The general appearance of the spectrum coincides with our previous results [8].

The study of the products of the interaction of CO with ZnO (Fig. 9) under various conditions showed that with an increase in the initial pressure of CO by two times, the areas of the peaks of CO and $CO_2$ (curves *1, 2* in Fig. 9) grow differently: the peak of CO increases approximately 3 times, and $CO_2$ — 1.5 times. However, the sum of the peak areas of CO and $CO_2$ doubles. This means that with such pre-processing of the sample (sec. 2) CO adsorption occurs mainly on Zn cations with the formation of weakly bound forms of Zn−CO, which can be removed by heating up to 400 K. The position of the peak of CO desorption after dark reactions does not change (curves *1–3* in Fig. 9), and the position of the peak $CO_2$ depends on the degree of coverage: the peak maximum shifts towards lower temperatures with increasing coverage (curves *1* and *2* in Fig. 9). This maximum shift is usually characteristic of associative desorption or desorption from an heterogeneous surface.

It can be seen from Fig. 9 that the largest amount of $CO_2$ is thermodesorbed after the dark interaction of a mixture of NO + CO with ZnO (curve *3*). This means that NO contributes to the formation of $O^-$ centers for the adsorption of CO [8]:

$$\mathrm{NO_{(ads)}} + \mathrm{Zn^+(e^-)} \rightarrow \mathrm{NO^-} + \mathrm{Zn^{2+}}, \tag{9}$$

$$\mathrm{NO^-} + \mathrm{NO} \rightarrow \mathrm{N_2O} + \mathrm{O^-}, \tag{10}$$

$$\mathrm{CO} + \mathrm{O^-} \rightarrow \mathrm{CO_2^-} \rightarrow \mathrm{CO_2} \uparrow + \mathrm{Zn^+(e^-, F^+)}. \tag{11}$$

The adsorption of CO leads to the reduction of ZnO, which is confirmed, in particular, by the acceleration of the formation of $N_2O$ (Fig. 6) and the generation of surface oxygen vacancies $V_O$ (F-centers) [8]. Thus, when interacting with the CO molecule, surface adsorbed and structural oxygen $O^-$ is removed. The electrons generated during the formation of the oxygen vacancy $V_O$ are localized on zinc cations ($Zn^+$) and/or on the vacancy itself, forming $F^+$-centers active in the adsorption of NO.

A noticeable increase in the amount of $CO_2$ (curve *3* in Fig. 9, 10) is explained by the appearance of additional $O^-$ centers as a result of the reaction (5). These facts are confirmed, among other things, by the material balance equation for CO and $CO_{2(\mathrm{ads})}$: adding CO to NO leads to additional adsorption of $\Delta\mathrm{NO} = 0.7 \cdot 10^{17}$ molecules, adding NO to CO, in turn, leads to the appearance of $\Delta\mathrm{CO}_{2(\mathrm{ads})} = 0.69 \cdot 10^{17}$ compared to the TD spectrum of the dark interaction of CO with ZnO (Fig. 9).

In the TD spectrum of reaction products (1) the form of the main peak of $CO_2$ ($T \approx 730\,\mathrm{K}$) is close to symmetric, which indicates the predominance of associative desorption. The peak is satisfactorily (a coincidence of $\approx 95\%$ match) modeled by a second-order monopik with parameters $\nu = 10^{12}\ \mathrm{s^{-1}}$, $\beta = 20\,\mathrm{K/min}$ and desorption activation energy $E_{\mathrm{des}} = 2.47\,\mathrm{eV}$, which indicates the energy uniformity of the surface with respect to the adsorption of $CO_2$. The difference between the experimental and model spectra of $CO_2$ is also shown in Fig. 11. The resulting peak has an asymmetric shape characteristic of first-order thermal desorption, but its half-width exceeds that for a uniform surface.

Comparing the TD spectra after irradiation of $\mathrm{ZnO/ZnO_{1-x}/O^-}$ in a mixture of $\mathrm{NO + CO} + 382\,\mathrm{nm}$ (Fig. 11) and after dark interaction of a mixture of NO + CO with $\mathrm{ZnO/ZnO_{1-x}/O^-}$ (Fig. 10) with the spectra of Fig. 8, it can be concluded that the addition of CO reduces the intensity of high-temperature peaks of NO both in the dark and during illumination.

## 5. Conclusion

For the first time, an exciton activation channel of the ecologically important photocatalytic reaction $\mathrm{NO + CO} \xrightarrow{h\nu} \mathrm{CO_2} + 1/2\ \mathrm{N_2}$ was used on ZnO. The efficiency of the exciton excitation channel was shown by us earlier [10] on the example of a model redox reaction of the POIE. However, the POIE reaction proceeds in the binary system $\mathrm{ZnO-O_2}$ and the question remains — will the activity of the photocatalyst remain in the atmosphere of a real reaction mixture? The experiments carried out in this paper gave a positive answer to this question. This makes it possible to recommend the $\mathrm{ZnO/ZnO_{1-x}/O^-}$ system for for air purification in closed spaces using highly efficient resonant LED light sources emitting in the exciton region of ZnO to activate the photocatalyst.

## Appendix

$$\mathrm{NO_{ads}} + \mathrm{Zn^+} \rightarrow \mathrm{NO^-} + \mathrm{Zn^{2+}}, \tag{П1}$$

$$\mathrm{NO^-_{(a)}} + \mathrm{NO} \rightarrow \mathrm{N_2O} + \mathrm{O^-}, \tag{П2}$$

$$\mathrm{N_2O} + \mathrm{Zn^+(e^-)} \rightarrow \mathrm{N_2} + \mathrm{O^-} + \mathrm{Zn^{2+}}, \tag{П3}$$

$$\mathrm{O^-} + \mathrm{NO_{(ads)}} \rightarrow \mathrm{NO^-_{2(ads)}}. \tag{П4}$$

The form $NO^-_{2(ads)}$ appears in the corresponding TD spectrum as a high-temperature ($T = 750-760$ K) peak,

$$3NO + O^{2-} \rightarrow N_2O + NO^-_2 + NO^-_3. \qquad (П5)$$

In the processes (P1), (P3)–(P5), electron-donor centers create the forms $NO^-$, $NO^-_2$, $NO^-_3$. In addition, weakly bound nitrosyl complexes Zn–NO are formed, forming bands in the IR spectra at 1915 and 1900 $cm^{-1}$. These strips are removed by evacuation at room temperature. The total reaction is written as

$$Zn^+(e^-) + 3NO_{(ads)} \rightarrow Zn^{2+} + NO^-_{2(ads)} + N_2O. \qquad (П6)$$

Formation on the surface of $CO^-_2$ and $CO^-_3$ in the process of illumination, it can also be represented by the interaction of CO with the hole center $O^-$:

$$O^- + CO \rightarrow CO^-_2, \qquad (П7)$$

$$O^- + CO \rightarrow (CO_2)_{ads} + V_O(F^+), \qquad (П8)$$

where $V_O(F^+)$ — a once charged anionic vacancy.

A recharge is possible $CO^-_2$:

$$CO^-_2 + Zn^{2+} \rightarrow Zn^+ + (CO_2)_{ads}. \qquad (П9)$$

In turn, the carboxylate complex $CO^-_2$ can be formed as a result of interaction with $Zn^+$ or the complex $CO^-_3$ [19] as a result of the interaction with a hole center:

$$(CO_2)_{ads} + Zn^+ \leftrightarrow CO^-_2 + Zn^{2+}, \qquad (П10)$$

$$(CO_2)_{ads} + O^- \rightarrow CO^-_3. \qquad (П11)$$

The above-mentioned structures of carbon oxides are firmly bound to the surface and are removed only at 750–800 K. At the same time, the TD spectra demonstrate weakly bound carbonyl groups $Zn^+$–CO on the illuminated surface, which are removed by evacuation at room temperature. And these are the structures that react at the first stage.

### Acknowledgments

The study was carried out with the support of the centers „Nanocomposites“, „Physical Methods of Surface Investigation“, „X-ray Diffraction Center“ and „Nanophotonics“ St. Petersburg State University. The authors thank A.A. Lisachenko and L.L. Basov for their help in the work and valuable discussions.

### Funding

RFBR Grant No. 18-03-00754.

### Conflict of interest

The authors declare that they have no conflict of interest.

## References

[1] Chong-Chen Wang, Jian-Rong Li, Xiu-Liang Lu, Yan-Qiu Zhang, Guangsheng Guo. Energy Environ. Sci., **7**, 2831 (2014). DOI: 10.1039/c4ee01299b
[2] U. Ozgur, Y.I. Alivov, C. Liu, A. Teke, M.A. Reshchikov, S. Dogan, V. Avrutin, S.J. Cho, H. A. Morkoç. J. Appl. Phys., **98**, 041301 (2005). DOI:?10.1063/1.1992666
[3] M. Law, L.E. Greene, J.C. Johnson. Nature Materials, **4** (6), 455–459 (2005). DOI:10.1038/nmat1387
[4] S. Rehman, R. Ullah, A.M. Butt, N.D. Gohar. J. Hazardous. Materials, **170**, 560–569 (2009). DOI:?10.1016/j.jhazmat.2009.05.064
[5] A. Kołodziejczak-Radzimska, T. Jesionowski. Materials, **7**, 2833–2881 (2014). DOI:10.3390/ma7042833
[6] Yajun Wang, Qisheng Wang, Xueying Zhan. Nanoscale, **5**, 8326 (2013). DOI: 10.1039/c3nr01577g
[7] V.E. Drozd, V.V. Titov, I.A. Kasatkin, L.L. Basov, A.A. Lisachenko, O.L. Stroyuk, S.Y. Kuchmiy. Thin Solid Films, **573**, 128–133 (2014). DOI: 10.1016/j.tsf.2014.11.023
[8] I.V. Blashkov, L.L. Basov, A.A. Lisachenko. J. Phys. Chem. C, **121**, 28364–28372 (2017). DOI:?10.1021/acs.jpcc.7b10143
[9] A. A. Lisachenko, L.L. Basov. In: *Book of Abstracts, 25th International Conference on Defects in Semiconductors (ICDS-25)* (Saint-Petersburg, 2009), p. 363.
[10] V.V. Titov, A.A. Lisachenko, M.E. Labzovskaya, I.Kh. Akopyan, B.V. Novikov. J. Phys. Chem. C, **123**, 27399–27405 (2019). DOI:?10.1021/acs.jpcc.9b08507
[11] E.F. Gross, N.A. Karryev. DAN SSSR, **84** (3), 471–474 (1952). (in Russian).
[12] A.N. Terenin. *Fotonika molekul krasiteley i rodstvennykh organicheskikh soedineniy.* (Nauka, Leningrad, 1967), p.498. (in Russian).
[13] V.V. Titov, A.A. Lisachenko, M.E. Labzovskaya, I.Kh. Akopyan, B.V. Novikov. Phys. Sol. State, **61** (11), 2134–2138 (2019). DOI:?10.1134/S1063783419110398
[14] R.V. Mikhaylov, A.A. Lisachenko, V.V. Titov. J. Phys. Chem. C, **116**, 23332–23341 (2012). DOI:?10.1021/jp305652p
[15] V.V. Titov, A.A. Lisachenko, I.K. Akopyan, M.E. Labzowskaya, B.V. Novikov. J. Lumin., **195**, 153–158 (2018). DOI: 10.1016/j.jlumin.2017.11.022
[16] A.A. Lisachenko, A.O. Klimovskii, R.V. Mikhailov, B.N. Shelimov, M. Che. Appl. Catalysis B: Environmental, **67**, 127–135 (2006). DOI: 10.1016/j.apcatb.2006.04.018
[17] R.V. Mikhaylov, A.A. Lisachenko, B.N. Shelimov, V.B. Kazansky, Gianmario Martra, Salvatore Coluccia. Phys. Chem. C, **20** (117), 10345–10352 (2012). DOI:?10.1021/jp311593s
[18] R.V. Mikhaylov, A.A. Lisachenko, B.N. Shelimov, V.B. Kazansky. J. Phys. Chem. C, **113**, 20381–20387 (2009), DOI: 10.1021/jp906176c
[19] D. Scarano, G. Spoto, S. Bordiga, A. Zecchina. Surface Science, **276**, 281–298 (1992). DOI:?10.1016/0039-6028(92)90716-J
[20] J. Raskó, F. Solymosi. J. Phys. Chem., **98**, 7147–7152 (1994). DOI:?10.1021/j100080a009